Supporting Information

Hydrangea-like Superstructured Micro/Nanoreactor of Topotactically Converted Ultrathin Bismuth Nanosheets for Highly Active CO_2 Electroreduction to Formate

Chan-Juan Peng,[†,‡] *Guang Zeng*,[†] *Dong-Dong Ma*,[†] *Changsheng Cao*,[†,‡] *Shenghua Zhou*,[†,‡] *Xin-Tao Wu*[†,§] and *Qi-Long Zhu**,[†,‡,§]

[†]State Key Laboratory of Structural Chemistry, Fujian Institute of Research on the Structure of Matter, Chinese Academy of Sciences, Fuzhou 350002, China

[‡]University of Chinese Academy of Sciences, Beijing 100049, China

[§]Fujian Science & Technology Innovation Laboratory for Optoelectronic Information of China, Fuzhou 350108, China

*Corresponding author: E-mail: qlzhu@fjirsm.ac.cn

Chemical and Materials: All reagents and chemicals are analytical grade. Glycerol ($C_3H_8O_3$, AR), N,N-dimethylformamide (DMF, AR), ethanol (C_2H_5OH, AR), bismuth nitrate ($Bi(NO_3)_3 \cdot 5H_2O$, AR, 99%), potassium bicarbonate ($KHCO_3$, 99.99%), potassium hydroxide (KOH, 99.99%), commercial Bi nanopowders (Bi, 99.99%) and dimethylsulfoxide (DMSO, 99.95%) were purchased from Alfa Aesar. Nafion (5 wt%) and deuteroxide (D_2O, 99.9%), were purchased from Sigma-Aldrich. Carbon paper was got from Toray Industries Inc.

Preparation of $(BiO)_2CO_3$ nanosheets: $(BiO)_2CO_3$ was synthesized using a solvothermal method. $Bi(NO_3)_3 \cdot 5H_2O$ (1 mmol) and urea (50 mmol) were dissolved in alcohol and H_2O (40 mL, v/v 1:1) to form an uniform solution by stirring for 30 min. Subsequently, the above mixture was heated at 90 °C for 4 h in oil bath. After reaction, the precipitate was washed with large amount of ethanol and de-ionized water by centrifugation to remove impurities, and then dried at 60 °C for 6 h in a vacuum.

Preparation of Bi-NSs: Typically, the material slurry was obtained by mixing $(BiO)_2CO_3$ (10 mg), H_2O (700 μL), DMF (200 μL) and 5 wt% Nafion solution (100 μL) under ultrasonic treatment for 2 h. Then 50 μL of the slurry was loaded to the both sides of a carbon paper (1.0×1.0 cm^2) and then dried in air to get a mass loading of 0.5 mg cm^{-2}. The as-prepared $(BiO)_2CO_3$ electrode was underwent repeated cyclic voltammetry cycles at 50 mV s^{-1} between –0.9 and –1.8 V (*vs.* Ag/AgCl) for 16 cycles in CO_2-saturated 0.5 M $KHCO_3$ electrolyte.

Characterization methods: The crystal structures were examined by powder X-Ray diffraction (PXRD) on an X-ray diffraction instrument Rikagu Miniflex 600 Benchtop with Cu K_α radiation (λ = 0.154 nm) and a counting time of 30 s per step. The morphologies and structures were identified by scanning electron microscopy (SEM, JEOL JSM-7800F, Hitachi, Krefeld, Germany) at 20 kV. Transmission electron microscopy (TEM) and high-resolution TEM (HRTEM) images were collected by FEI Tecnai G2 F30 working at 200 kV. The X-ray

photoelectron spectroscopy (XPS) experiments were obtained on a Thermo Fischer ESCALAB 250Xi X-ray photoelectron spectrometer using an Al Kα X-ray radiation (E = 1486.2 eV). The thickness of the samples was tested by atomic force microscopy (AFM) in an atomic force microscope (Bruker Dimension ICON).

Electrochemical measurements: The electrochemical measurements of the catalysts were conducted on a CHI 760 electrochemical workstation with a standard three-electrode system in a H-type electrochemical cell. The two chambers were separated by a proton-conducting membrane, which can prevent the cathodic products oxidized. A saturated Ag/AgCl electrode and Pt-mesh were applied as reference and counter electrodes, respectively. CO_2-saturated 0.5 M $KHCO_3$ (pH $\approx$7.2) served as the electrolyte. The cathodic chamber was directly connected to a gas chromatography spectrometer for product analysis. All the measured potentials were converted to the reversible hydrogen electrode (RHE) in this whole work ($E(RHE) = E(Ag/AgCl) + 0.059\times pH + 0.197\ V$).

The electrolytes were bubbled with CO_2 or Ar for 8 min to get CO_2 or Ar-saturated aqueous $KHCO_3$ solution (0.5 M) before the measurements. Linear sweep voltammetry (LSV) measurement were recorded at a scan rate of 10 mV min^{-1}. The double-layer capacitances (C_{dl}) was obtained based on Cyclic voltammetry (CV) curves. Specifically, CV experiment was performed with the potential range from 0.02 to 0.12 V to ensure nonoccurrence Faradaic processes at different scan rates. The electrochemical impedance spectroscope (EIS) was obtained at –0.83 V in a frequence from 100 mHz to 100 kHz at the AC amplitude of 5 mV. The Tafel slope was calculated by i-t curves and $FE_{formate}$ with a plot of potential *vs.* the logarithm of $j_{formate}$.

Computational methods: In our work, DFT calculations were carried out through the Vienna ab initio simulation package (VASP). The projector augmented wave (PAW) method was adopted to describe the interactions between ions and electrons. We used the generalized

gradient approximation (GGA) in the form of Perdew-Burke-Ernzerhof (PBE) exchange-correlation functional. The plane-wave basis set along with a kinetic cutoff energy was 400 eV. The Brillouin zones were sampled with 3 × 3 × 1 Monkhorst-Pack meshes. The structures were fully relaxed until the maximum force on each atom was less than –0.02 eV/Å and 10^{-5} eV. We investigated the CO_2RR progress of on the (0 1 2) plane of Bi-ene with the supercell of 3 × 4 × 1 unit cells. 6 atomic layers with the bottom 2 atomic layers are fixed along the z direction were built, and the 15 Å vacuum space was considered to avoid the periodic interaction along the *y* and *z* directions.

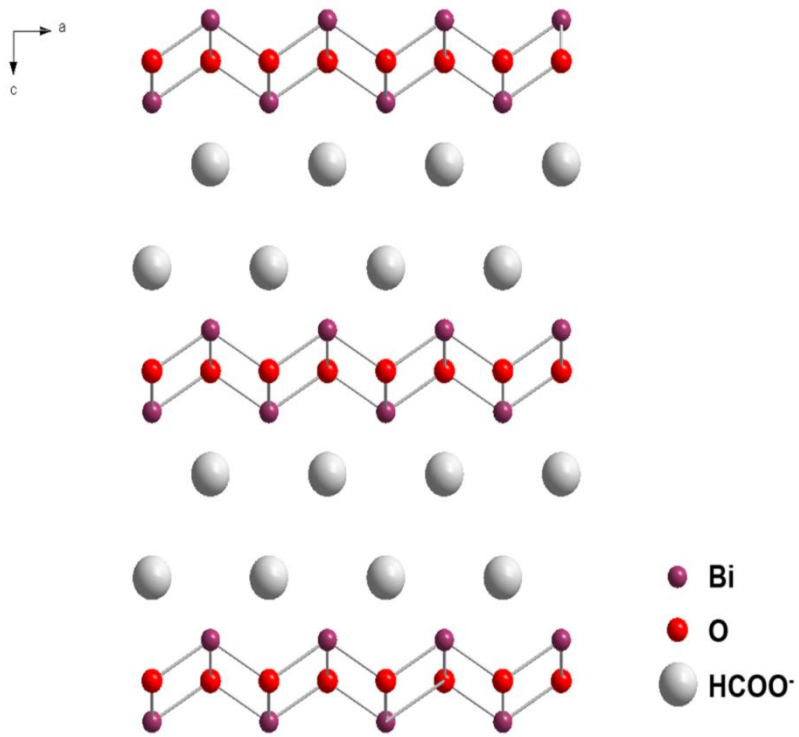

Figure S1. The crystal structure diagram of BiOCOOH.

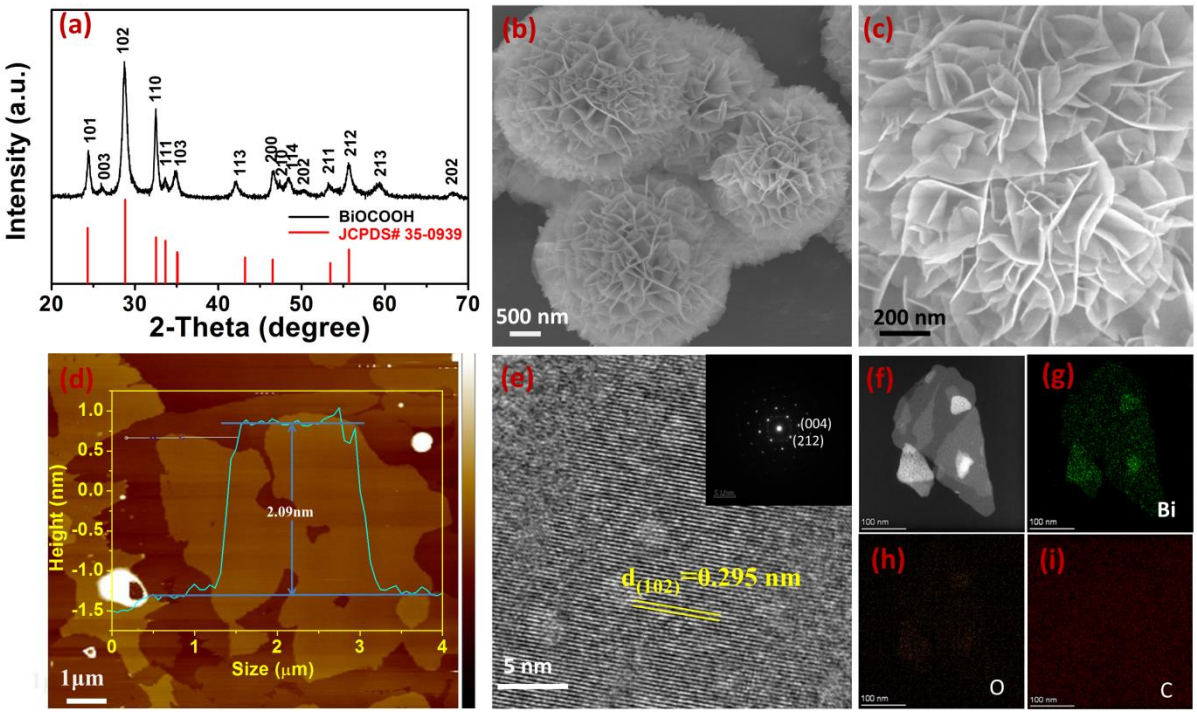

Figure S2. Characterizations of BiOCOOH. **(a)** PXRD, **(b, c)** SEM, **(d)** AFM, **(e)** HRTEM and **(f-i)** EDX elemental mapping images of BiOCOOH. Inset in **(e)** is the selected-area electron-diffraction (SAED) pattern of BiOCOOH.

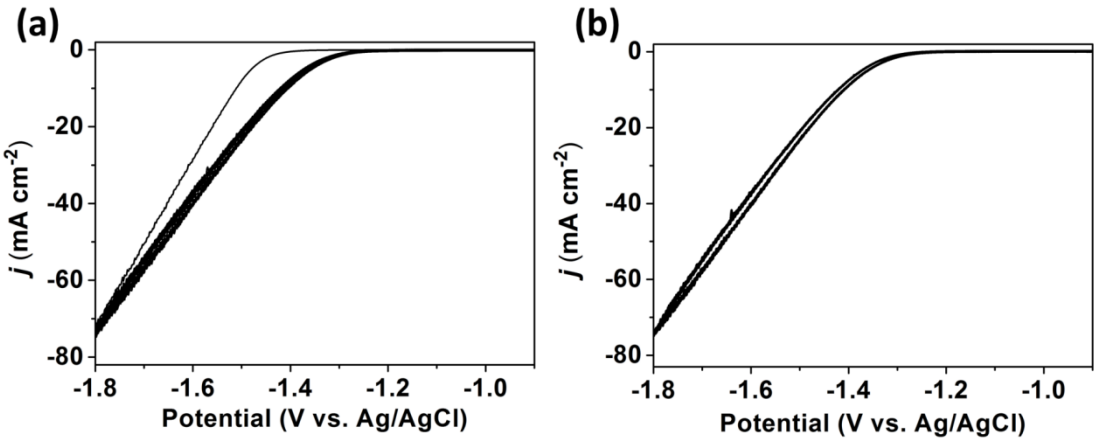

Figure S3. *In situ* electrochemical transformation of BiOCOOH to S-Bi-NSs. CV curves of BiOCOOH for first 16 cycles **(a)** and **(b)** followed 8 cycles.

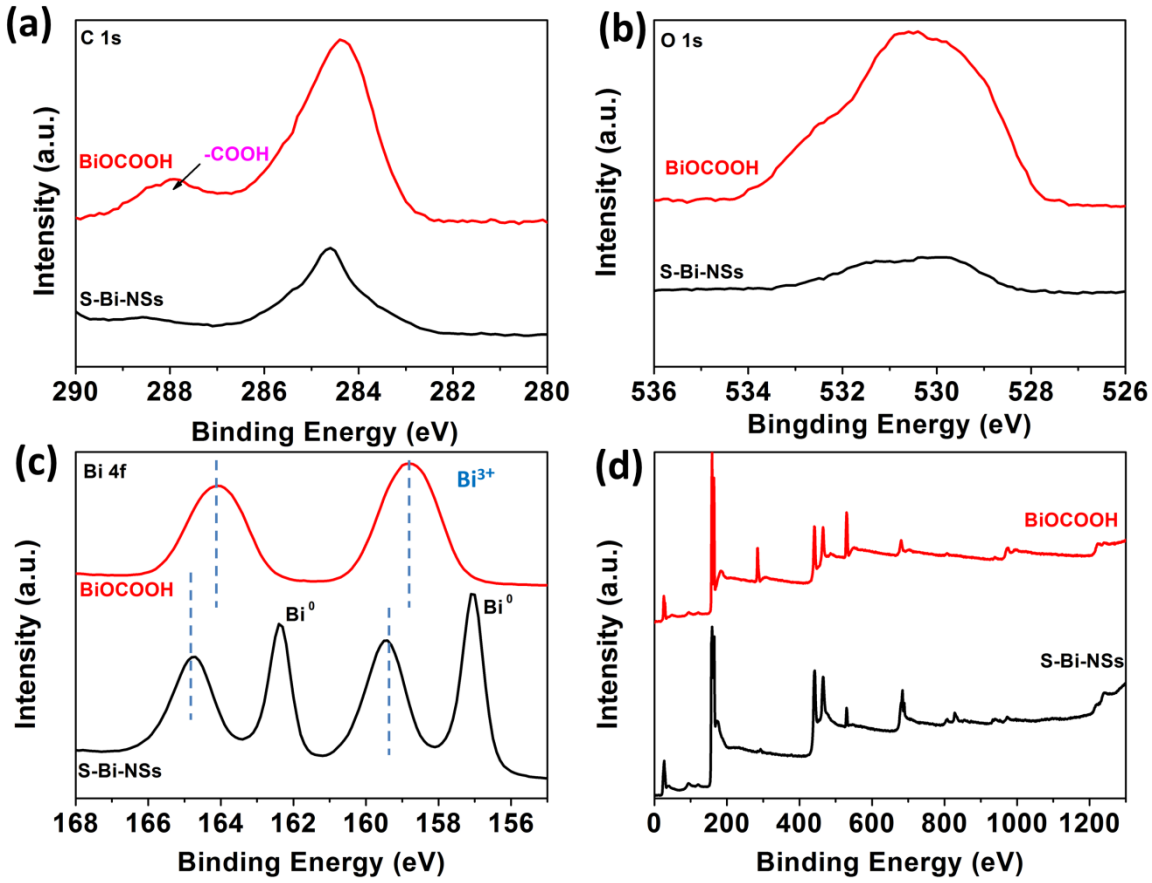

Figure S4 XPS spectra of BiOCOOH and S-Bi-NSs. **(a)** C 1s, **(b)** O 1s, **(c)** Bi 4f and **(d)** survey XPS spectra of BiOCOOH and S-Bi-NSs.

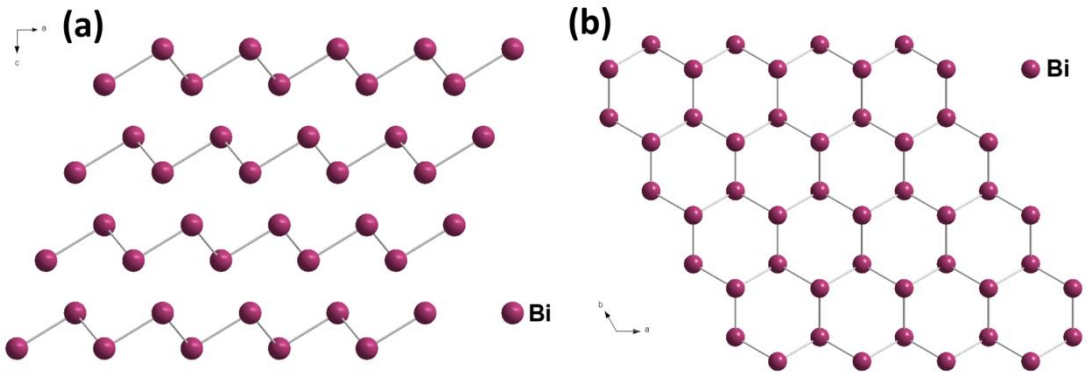

Figure S5. **(a,b)** The crystal structure diagram of metallic Bi.

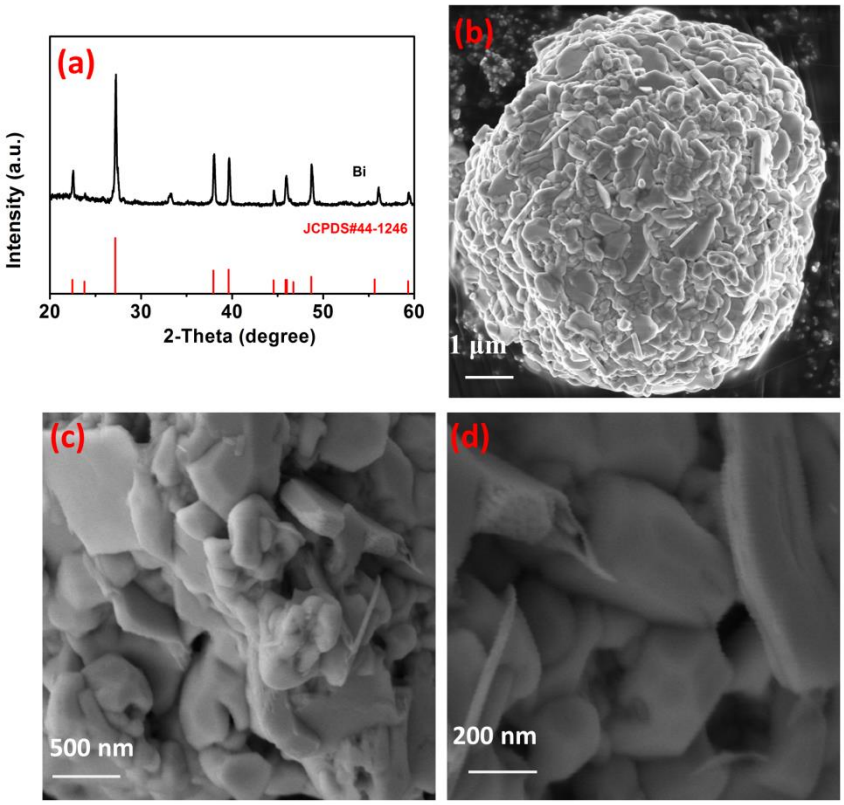

Figure S6. **(a)** PXRD pattern and **(b-d)** SEM images of the Bi nanopowders.

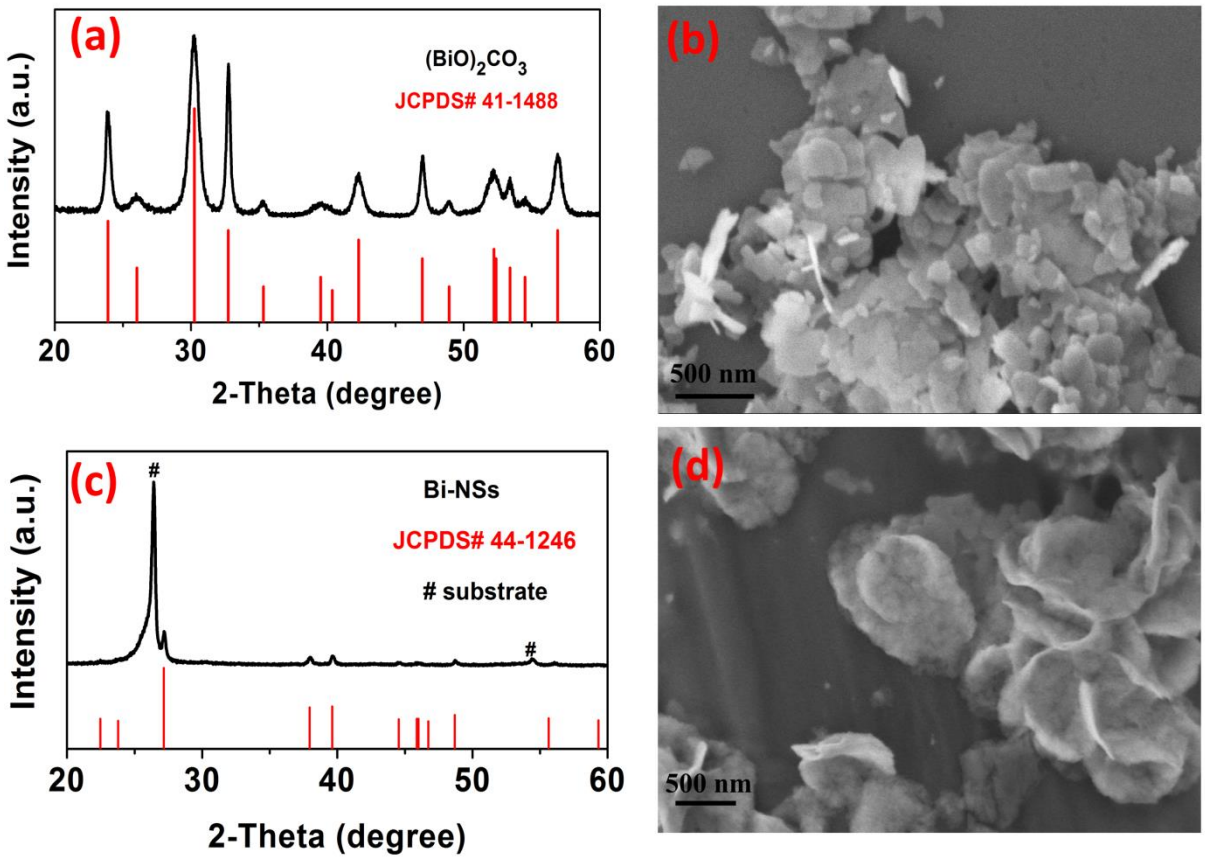

Figure S7. **(a,c)** PXRD patterns and **(b,d)** SEM images of $(BiO)_2CO_3$ and Bi-NSs.

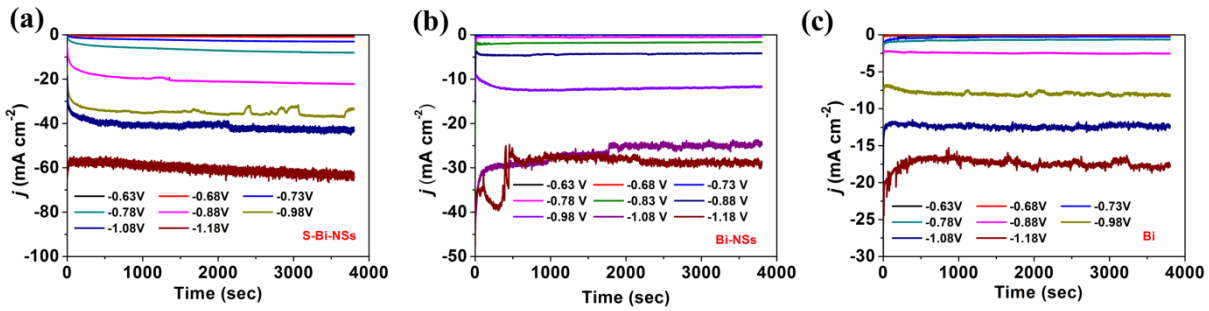

Figure S8. Current densities respect to time at given potentials for **(a)** S-Bi-NSs, **(b)** Bi-NSs, and **(c)** Bi nanopowders.

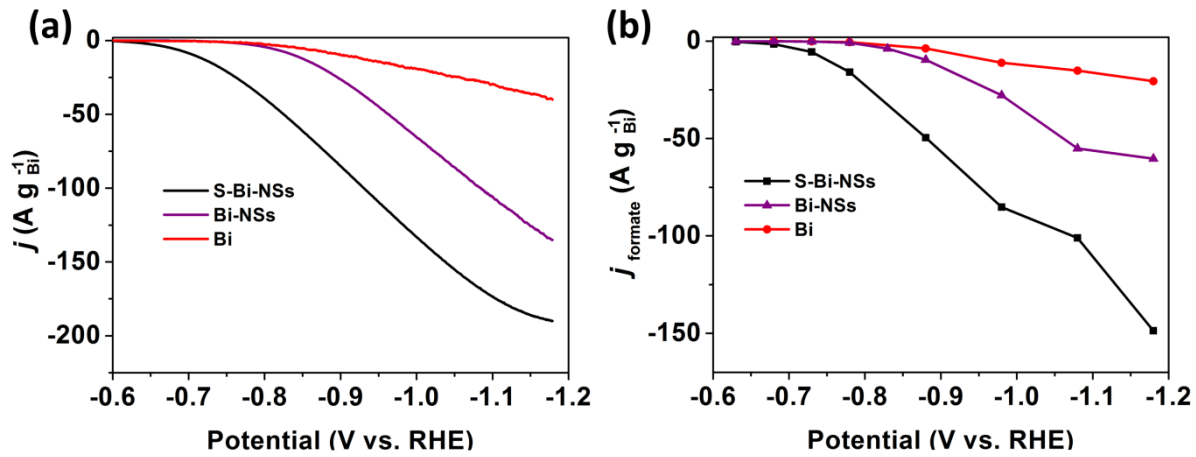

Figure S9. Comparison of the mass-specific CO_2RR performance of S-Bi-NSs, Bi-NSs and Bi nanopowders. **(a)** Total and **(b)** formate partial mass current densities.

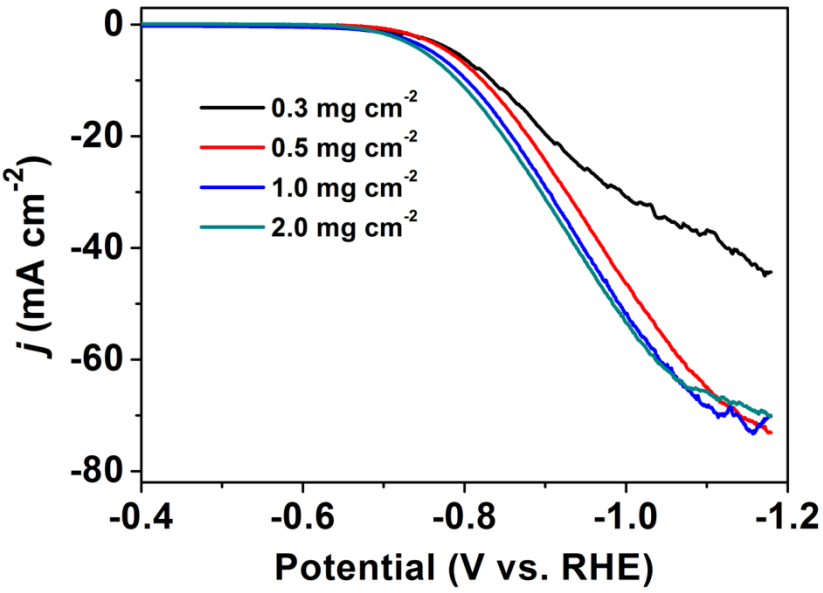

Figure S10. CO_2RR performance of S-Bi-NSs with different loadings (the marked loading values here are the loading amounts of the BiOCOOH precursor).

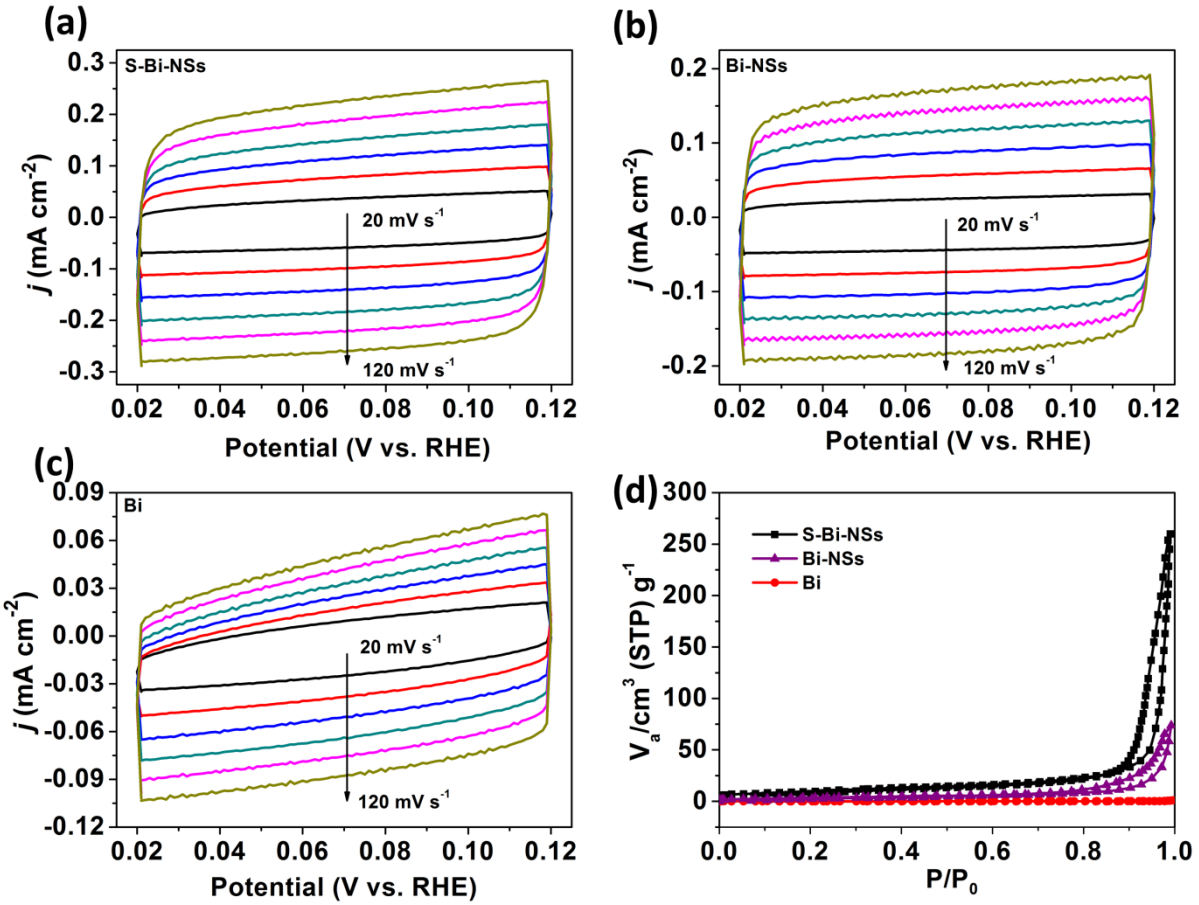

Figure S11. CV curves of **(a)** S-Bi-NSs, **(b)** Bi-NSs and **(c)** Bi nanopowders at different scan rates. **(d)** N_2 sorption isotherms of S-Bi-NSs, Bi-NSs and Bi nanopowders at 77 K.

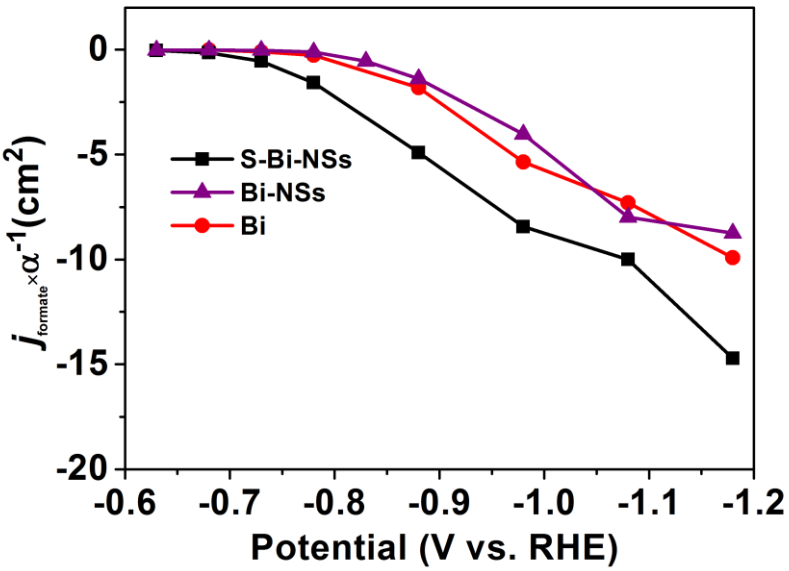

Figure S12. The formate partial current density normalized by ECSAs.

Table S1. Electrochemical CO_2 reduction properties of electrocatalysts for formate production.

Catalysts	Electrolyte	Potential (V vs. RHE)	$FE_{formate}$ (%)	Ref.
Commercial Bi	0.5 M $KHCO_3$	-0.88 V	78	
S-Bi-NSs	**0.5 M $KHCO_3$**	**-0.78 V** **-0.88 V** **-0.98 V** **-1.08 V** **-1.18 V**	**94** **95.3** **95.8** **96** **96**	**This work**
Bi-ene	0.5 M $KHCO_3$	-0.98 V	100	1
BiNS	0.5 M $NaHCO_3$	-0.95 V	100	2
Cu foam@BiNW	0.5 M $KHCO_3$	-0.99 V	95	3
Bi dendrite	0.5 M $KHCO_3$	-0.74 V	89	4
Bi_2O_3NSs@MCCM	0.1 M $KHCO_3$	-1.26 V	93.8	5
Bismuth particle	0.5 M $KHCO_3$	-0.83 V	94.7	6
Bi nanosheets	0.1 M $KHCO_3$	-1.1 V	86	7
Nano Bi	0.5 M $KHCO_3$	-1.6 Vvs.SCE	98.4	8
Oxide-derived Bi	0.5 M $KHCO_3$	-1.82 V	82	9
Shape-controlled Bi	0.1 M $KHCO_3$	-0.6 V	100	10
HSA-Bi	0.5 M $KHCO_3$	-1.5 V vs.SCE	92	11
Bi_{45}/GDE	0.5 M $KHCO_3$	-1.45 V vs.SCE	90	12
Reduced mpBi nanosheets	0.5 M $NaHCO_3$	-0.9 V	99	13
POD-Bi	0.5 M $KHCO_3$	-1.16 V	95	14
Nano-Bi/Cu	0.1 M $KHCO_3$	-0.88 V	91.3	15
Bi-NRs@NCNTs	0.1 M $KHCO_3$	-0.9 V	90.9%	16
Coralline $Ag_{65}Cu_{35}$	0.1 M $KHCO_3$	-1.0 V	91.8	17

Table S2. The obtained R_s and R_{ct} of bulk Bi, Bi-NSs and S-Bi-NSs.

	Bi	Bi-NSs	S-Bi-NSs
R_s/ Ω	2.4	2.1	2.3
R_{ct}/ Ω	62.85	7.9	5.1

REFERENCES

1. Cao, C.; Ma, D. D.; Gu, J. F.; Xie, X.; Zeng, G.; Li, X,; Han, S. G.; Zhu, Q. L.; Wu, X. T.; Xu, Q., Metal–Organic Layers Derived Atomically Thin Bismuthene for Efficient Carbon Dioxide Electroreduction to Liquid Fuel. *Angew. Chem. Int. Ed.* **2020**, *59*, 15124-15130.

2. Han, N.; Wang, Y.; Yang, H.; Deng J.; Wu, J.; Li, Y.; Li, Y., Ultrathin Bismuth Nanosheets From In Situ Topotactic Transformation for Selective Electrocatalytic CO_2 Reduction to Formate. *Nat. Commun.* **2018**, *9*, 1320-1328.

3. Zhang, X.; Sun, X.; Guo, Si.; Alan, b.; Zhang, J., Formation of Lattice-Dislocated Bismuth Nanowires on Copper Foam for Enhanced Electrocatalytic CO_2 Reduction at Low Overpotential. *Energy Environ. Sci.* **2019**, *12*, 1334-1340.

4. Koh, J. H.; Won, D.; Eom, T.; Kim, N.; Jung, K. D.; Kim, H.; Hwang, Y. J.; Ming, B. K., Facile CO_2 Electro-Reduction to Formate via Oxygen Bidentate Intermediate Stabilized by High-Index Planes of Bi Dendrite Catalyst. *ACS Catal.* **2017**, *7*, 5071-5077.

5. Liu, S.; Lu, X. F.; Xiao, J.; Wang, X.; Lou, X. W. D., Bi_2O_3 Nanosheets Grown on Multi-Channel Carbon Matrix to Catalyze Efficient CO_2 Electroreduction to HCOOH. *Angew. Chem. Int. Ed.* **2019**, *58*, 13828-13833.

6. Zhang, X.; Hou, X.; Zhang, Q.; Cai, Y.; Liu, Y.; Qiao, J., Polyethylene Glycol Induced Reconstructing Bi Nanoparticle Size for Stabilized CO_2 Electroreduction to Formate. *J. Catal.* **2018**, *365*, 63-70.

7. Zhang, W.; Hu, Y.; Ma, Li; Zhu, G.; Zhao, P.; Xue, X.; Chen, R.; Yang, S.; Ma, J.; Liu, J.; Jin, Z., Liquid-Phase Exfoliated Ultrathin Bi Nanosheets: Uncovering the Origins of Enhanced Electrocatalytic CO_2 Reduction on Two-Dimensional Metal Nanostructure. *Nano Energy* **2018**, *53*, 808-816.

8. Qiu, Y.; Du, J.; Dong, W.; Dai, C.; Tao, C., Selective Conversion of CO_2 to Formate on a Size Tunable Nano-Bi Electrocatalyst. *J. CO_2 Util.* **2017**, *20*, 328-335.

9. Bertin, E.; Garbarino, S.; Roy, C.; Kazemi, S.; Guay, D., Selective Electroreduction of CO_2 to Formate on Bi and Oxide-Derived Bi Films. *J. CO_2 Util.* **2017**, *19*, 276-283.

10. Kim, S.; Dong, W. J.; Gim, S.; Sohn, W.; Park, J. Y.; Yoo, C. Jang, H. W.; Lee, J., Shape-Controlled Bismuth Nanoflakes as Highly Selective Catalysts for Electrochemical Carbon Dioxide Reduction to Formate. *Nano Energy* **2017**, *39*, 44-52.

11. Zhang, H.; Ma, Y.; Quan, F.; Huang, J.; Jia, F.; Zhang, L., Selective Electro-Reduction of CO_2 to Formate on Nanostructured Bi From Reduction of BiOCl Nanosheets. *Electrochem. Commun.* **2014**, *46*, 63-66.

12. Zhang, X.; Lei, T.; Liu, Y.; Qiao, J., Enhancing CO_2 Electrolysis to Formate on Facilely Synthesized Bi Catalysts at Low Overpotential. *Appl. Catal. B: Environ.* **2017**, *218*, 46-50.

13. Yang, H.; Han, N.; Deng, J.; Wu, J.; Wang, Y.; Hu, Y.; Ding, P.; Li, Y.; Li, Y.; Lu, J., Selective CO_2 Reduction on 2D Mesoporous Bi Nanosheets. *Adv. Energy Mater.* **2018**, *8*, 1801536.

14. He, S.; Ni, F.; Ji, Y.; Wang, L.; Wen, Y.; Bai, H.; Liu, G.; Zhang, Y.; Li, Y.; Zhang, B.; Peng, H., The p-Orbital Delocalization of Main-Group Metals to Boost CO_2 Electroreduction. *Angew. Chem. Int. Ed.* **2018**, *57*, 16114-16119.

15. Lv, E.; Zhou, J.; Bei, J.; Zhang, R.; Wang, L.; Xu, Q.; Wang, W., Electrodeposition of Nano-Sized Bismuth on Copper Foil as Electrocatalyst for Reduction of CO_2 to Formate. *Applied Surf. Sci.* **2017**, *393*, 191-196.

16. Zhang, W.; Yang, S.; Jiang, M.; Hu, Y.; Hu, C.; Zhang, X.; Jin, Z., Nanocapillarity and Nanoconfinement Effects of Pipet-Like Bismuth@Carbon Nanotubes for Highly Efficient Electrocatalytic CO_2 Reduction. *Nano Lett.* **2021**, *21*, 2650-2657.

17. Zhang, W.; Xu, C.; Hu, Y.; Yang, S.; Ma, L.; Wang, L.; Zhao, P.; Wang, C.; Ma, J.; Jin, Z., Electronic and Geometric Structure Engineering of Bicontinuous Porous Ag–Cu Nanoarchitectures for Realizing Selectivity-Tunable Electrochemical CO_2 Reduction. *Nano Energy* **2020**, *73*, 104796.